Contents lists available at ScienceDirect

Chemical Engineering Journal

journal homepage: www.elsevier.com

Calcium alginate beads motion in a foaming three-phase bubble column

Gabriel Salierno[a], Mauricio Maestri[a], Stella Piovano[a], Miryan Cassanello[a, *], María Angélica Cardona[b], Daniel Hojman[b], Héctor Somacal[b, c]

[a] Laboratorio de Reactores y Sistemas para la Industria–LARSI, Dep. Industrias, FCEyN, Universidad de Buenos Aires, Int. Güiraldes 2620, C1428BGA Buenos Aires, Argentina
[b] Laboratorio de Diagnóstico por Radiaciones–LADiR, Dep. de Física Experimental, Comisión Nacional de Energía Atómica (CNEA), San Martín, Buenos Aires, Argentina
[c] Escuela de Ciencia y Tecnología, Universidad Nacional de San Martín, Buenos Aires, Argentina

ARTICLE INFO

Article history:
Received 26 February 2017
Received in revised form 7 May 2017
Accepted 8 May 2017
Available online xxx

Keywords:
Bubble columns
Solid motion
Foaming system
Radioactive Particle Tracking
Calcium alginate beads

ABSTRACT

Calcium alginate beads are frequently used to immobilize enzymes or microorganisms for fermentations carried out in agitated or pneumatic reactors. In this work, the well-known Radioactive Particle Tracking (RPT) technique is used to non-invasively extract relevant information of the motion of calcium alginate beads within a three phase bubble column under foaming conditions, which frequently appear in bioreactors operation. Special care is taken to produce a radioactive tracer that perfectly matches the features of the other particles in density and size. In addition, the tracer has the same texture and wettability since the adherence of gas to particles in foaming systems is crucial in determining the solid motion. Particles distribution, solid residence time, velocity fields, dispersion coefficients, shear stress and turbulence kinetic energy are determined from the radioactive tracer trajectories. Compared to previous works in non-foaming systems with denser particles, a relatively strong inward flow and less definite descending motion of the solid near the column wall is found. Turbulence intensities and shear stress are high in the disengagement zone, particularly for the churn-turbulent flow regime. However, since the biocatalyst damage would also depend on the actual exposure to harsh regions, the frequency of visit at different location was calculated to estimate maps of exposure risks as the product of turbulence stresses and these frequencies. Considering the particles motion, the region of largest risk for hydrodynamic damage is close to the gas entrance zone.

1. Introduction

Immobilization is generally used in bioprocesses to protect biocatalyst from inhibitory products and harsh environment and, especially, to increase the catalyst concentration and facilitate its separation and recycling, thus improving bioreactors productivity [1,2]. Low density polysaccharide gel particles, such as alginate or carrageenan beads, are frequently used to immobilize enzymes or microorganisms for fermentations, since they provide ease of entrapment under mild conditions [3].

Fermentations with immobilized biocatalysts are generally carried out in vessels agitated mechanically or pneumatically with a circulating gas; the last are frequently three phase bubble columns [4]. Precision mixing in multiphase systems traditionally contributes to reduce costs of installed processes, and to increase safety margins and competitiveness of process to come [5]. There is a wide range of operating conditions where an imprecise control of process variables leads to decline the productivity and the operational capacity of bubble columns [6]. For example, knowing the motion of the substrates and cells in a bioprocess is crucial to select the design variables and operating conditions that ensure good mixing while minimizing the existence of stagnant regions and maintaining turbulence levels compatible with living organisms [7]. Cellular responses to turbulence can range from no effect to significant physiological or genetic effects and finally, apoptosis or rapid cell lysis [8]; even immobilized enzymes can be deactivated due to high levels of hydrodynamic stress [2]. On the other hand, algae cell membranes resistance to lysis is high and can be exposed to significant shear for improving light exposure [9], and high stirring speeds plus gas sparging can occasionally be beneficial for maximizing the desired product [10]. Therefore, more research is needed to increase the reliability of scaling up bioprocess equipment. Bioreactor design and scale up is one of the most important open problems of chemical engineering [11].

Bubble Columns (BCs) have some advantages over stirred tank reactors (STRs) for mitigating the hydrodynamic stress, such as more gentle and distributed shear stress, since they do not have a mixer or impeller. In addition, construction and scale-up imply lower costs [4]. However, the lack of an impeller also brings some disadvantages, such as poor fluid mixing for highly viscous culture compared to STR. An additional complexity is serious foaming under high aeration, often undesirable since foam is a vehicle for contamination and may even cause loss of liquid phase [12]. Even if foaming conditions are tried to be avoid, many times it is not possible in bioprocesses and foam is therefore destroyed by mechanical means in the upper region but exists in the bulk. Also, the addition of shear-protective agents may promote foam because it mitigates the influence of bubbles bursts. There are also some bioprocesses for which a foam outflow is used for product recovery (e.g., production of biosurfactants

* Corresponding author.
Email address: miryan@di.fcen.uba.ar (M. Cassanello)

http://dx.doi.org/10.1016/j.cej.2017.05.060
1385-8947/

or lipopeptides [13,14]). Since the motion of solids under foaming conditions has been very scarcely examined in the literature and could appear in several bioprocesses, further knowledge of this system dynamics may contribute to establish more reliable tools for bioreactor design, scale-up and operation.

The well-known Radioactive Particle Tracking (RPT) technique has been successfully applied to study two and three phase bubble columns [15–18] and more recently for air-lift bioreactors [19–21]. Although bubble columns solid dynamic has been intensively examined, scarce information is available in the open literature on the motion of deformable gel particles and less if they are moving in a foaming gas-liquid system. RPT experiments are one of the very limited techniques suitable for experimentally determining the motion of condensed solid in opaque systems to validate computational fluid dynamics (CFD) codes, which may be very helpful for bioreactor scale-up. It is worth mentioning also that RPT experiments provide an experimental estimation of the biocatalyst lifelines [22], which is a very interesting concept for establishing scale-up rules.

The aim of this work is to perform RPT experiments for gathering relevant information of the motion of calcium alginate beads, a typical immobilization support for biocatalysts, while suspended in a foaming gas-liquid system in a pilot scale bubble column. The adherence of gas bubbles to particles is crucial in determining their motion, particularly in foaming systems with low density particles. Hence, special care is taken to produce a radioactive tracer that perfectly matches the other particles texture and wettability, apart from size and density. The influence of the gas velocity on the solid velocity field, solid distribution, residence time, frequency of visit to different regions and turbulence parameters, is examined within a range covering the bubbling and the churn turbulent flow regimes. Column regions where the biocatalysts could be most damage are diagnose from the experiments.

2. Materials and methods

2.1. Experimental setup

Experiments have been carried out in a 1.2 m high and 0.1 m inner diameter acrylic column. Liquid and solid were in batch mode and mixed by circulating air. The gas distributor used was a perforated plate with 32 holes of 1 mm diameter, representing 0.32% of the column section. The gas distributor top is located in the base of the column ($z = 0$). The model liquid used was a 0.5 M $CaCl_2$ aqueous solution with added benzalkonium chloride (0.1 ppm) both as fungicide and to promote foaming. The solid inventory, calcium alginate beads of 5 mm mean diameter, were prepared by extrusion dripping of a 1.5% (w/v) sodium alginate aqueous solution onto a 0.5 M $CaCl_2$ solution using a peristaltic pump, to form the calcium alginate beads by ion exchange [3]. The procedure used to obtain the beads is the typical one for immobilizing a biocatalyst, either enzymes or cells, by retention. Particle size distribution, as determined from image analysis of captured photographs extracted from a video of the suspended beads, presents an almost normal shape with a coefficient of variance of around 20%. The solid inventory represented 10% v/v of the liquid. The solid-liquid mixture height at rest was 0.55 m. Gas superficial velocity was varied within the range of 0.021–0.095 m/s.

The motion of a radioactive tracer, representing the calcium alginate beads, was continuously followed (every 30 ms for several hours) by an array of sixteen 2 × 2 in. NaI(Tl) scintillators, located around the column as illustrated in the photograph of Fig. 1a; i.e., 4 lines (at $z = 120$, 320, 520 and 720 mm) of 4 detectors, separated 90° in between.

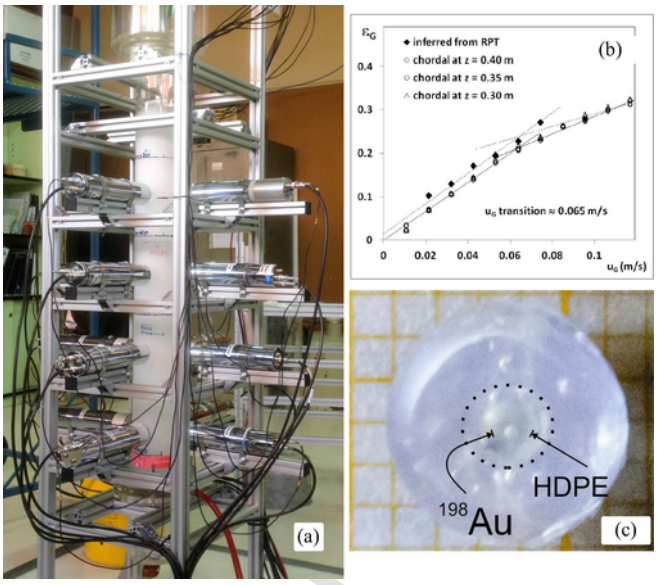

Fig. 1. Photograph of the RPT experimental installation (a); influence of the gas velocity on the chordal gas holdup determined by gamma densitometry and from the three-phase expansion inferred from the highest tracer axial positions, indicating the region of flow transition (b); photograph of the tracer (c).

Flow regime transition was evaluated from the trend in chordal gas holdup vs gas velocity determined by gamma densitometry experiments at three column heights (Fig. 1b). In addition, it was determined from statistical analysis of the tracer time series, and by visual inspection [23]. These complementary methods indicated that transition conditions are apparent for gas velocities in the range 0.055–0.066 m/s. Finally, for comparison, the gas holdup was also determined from the solid expansion inferred from the RPT experiments as the median of the 50 highest tracer axial coordinates for each experiment. Then, the liquid in the foam above the end of the three-phase emulsion was neglected and the gas holdup was estimated as the three-phase expansion minus the solid-liquid height at rest (zero gas velocity) divided by the three-phase expansion. Fig. 1b illustrates the comparison; although the absolute values of the gas holdup are slightly larger than those determined by densitometry, the flow regime transition velocity is fairly coincident. Hence, RPT experiments cover the homogeneous, transition and heterogeneous flow regimes; representative experimental results of each flow regime will be shown for discussion.

The tracer used to track the solid was prepared by embedding a high density polyethylene (HDPE) sphere containing a tiny piece of gold in a calcium alginate bead prepared resembling the rest of the particles in the bed (Fig. 1c). The gold embedded in HDPE was activated by neutron bombardment in the RA1 reactor of the National Commission of Atomic Energy in Argentina (CNEA), giving ^{198}Au ($t_{1/2} \approx 2.7$ d, Epeak = 412 keV) of around 50 μCi. The already activated tracer is then deposited inside matrices of half spheres designed for producing the calcium alginate bead tracer in three steps: i. – polymerization of one half of the gel bead and introduction of the particle in the middle, ii. – polymerization of the second half on top, iii. – reshaping of the bead in a $CaCl_2$ solution bath to improve the spherical shape and perfectly cover any separation. The resulting tracer is similar in size, density and texture as the alginate beads forming the bed. Further details of the tracer preparation method can be found in [23]. Size and density similarity of the tracer and the other prepared particles are verified by image analysis and by comparing their sedimentation velocity. Texture and wettability of the

tracer is similar to the particles forming the bed since the external part of the tracer is the same. The gel completely surrounds the inner HDPE sphere. Several tracers are produced and the best match is selected for the experiments.

The "instantaneous" tracer positions (every 30 ms) were reconstructed considering the photon counts simultaneously detected by the scintillators. The number of counts registered by each detector depended on the tracer intensity, the media attenuation and the detection system dead time. For the reconstruction, a calibration stage was performed; it consisted in measuring the counts while locating the tracer at known positions within the three-phase emulsion. Calibration points were located at several radial/azimuthal positions for several axial coordinates in the column covered by the three-phase emulsion within the range z = 70 mm to z = 820 mm. With the signal distribution measured when the tracer is located at the calibration points, parameters of a model based on MonteCarlo calculations were fitted for each detector by minimizing the difference between the counts measured and estimated, as described in [24]. This reconstruction procedure allows determination of tracer coordinates below the lowest and above the highest detectors to a certain distance. The ability of reconstruction was verified by comparing with known fixed positions in the column from the column base up to z = 820 mm. Using the fitted parameters and the model, a database of correspondence between positions within the reactor and signal distribution was created and used to get the tracer positions while freely moving within the emulsion.

From the long tracer trajectories, the probability of occurrence of the tracer at different regions within the column, which has been argued to be related to the local solid holdup [15,25] was determined. In addition, instantaneous velocities were calculated by direct differentiation of successive positions and assigned to a voxel containing the middle coordinates, for determining the solid 3D velocity fields. From the fluctuating velocities, calculated as the instantaneous minus the mean velocities, turbulent parameters were obtained [21,24]. Eq. (1) indicates the deformation tensor, τ, estimated considering the average of the product of fluctuating velocity components.

$$\tau = \rho \begin{bmatrix} \tau_{rr} & \tau_{\theta r} & \tau_{zr} \\ \tau_{r\theta} & \tau_{\theta\theta} & \tau_{z\theta} \\ \tau_{rz} & \tau_{\theta z} & \tau_{zz} \end{bmatrix} = \rho \begin{bmatrix} \langle u_1' u_1' \rangle & \langle u_1' u_2' \rangle & \langle u_1' u_3' \rangle \\ \langle u_2' u_1' \rangle & \langle u_2' u_2' \rangle & \langle u_2' u_3' \rangle \\ \langle u_3' u_1' \rangle & \langle u_3' u_2' \rangle & \langle u_3' u_3' \rangle \end{bmatrix} \quad (1)$$

where the subscripts 1, 2, 3 correspond respectively to the radial, r, azimuthal, θ, and axial, z, components of the fluctuating velocities u', and ρ is the fluid density. From the tensor, the turbulent kinetic energy (sum of normal stresses, evaluated as the trace, Eq. (2)) and the radial-axial shear stress (mixed product of the radial and axial components, Eq. (3)) were obtained for different locations in the column.

$$\mathrm{TKE} = \langle u_1' u_1' \rangle + \langle u_2' u_2' \rangle + \langle u_3' u_3' \rangle \quad (2)$$

$$\tau_{rz} = \langle u_1' u_3' \rangle \quad (3)$$

The solid dispersion coefficients were estimated considering the Einstein equation. For this calculation, it was assumed that extracts of the long tracer trajectory starting from given locations at delayed times represent different particles. Then, the derivatives of the mean square displacements of particles released from different initial positions (r_0, z_0) were used for computing the particles axial and radial dispersion coefficients, as expressed in Eq. (4) [24].

$$D_z = \frac{1}{2}\frac{d}{dt}\langle (z - z_0)^2 \rangle;\ D_r = \frac{1}{2}\frac{d}{dt}\langle (r - r_0)^2 \rangle \quad (4)$$

RPT is a powerful technique allowing estimations of the residence time distributions of solid particles at different locations in the column by considering the time that the tracer remains within given regions for different periods of the long tracer trajectories [25]. Hence, axial-radial maps (azimuthally averaged) of solid mean residence time are also reported for representative experiments. Finally, the frequency of visit of different column regions can be evaluated from the long tracer trajectories as the inverse of the mean time elapsed before the tracer reenters given locations. This frequency allows determination of the risk of exposure of the solid particles to regions of high hydrodynamic stress.

3. Results

3.1. Solid distribution and flow pattern

The normalized probabilities of tracer radial positions, calculated as the number of registrations of the tracer in each voxel divided by the total number of registrations on an equal volume value, are shown in Fig. 2, for three gas velocities at different column heights, and axially averaged. All over the column, there is a sharp decrease of the probability of solid occurrence for the region immediately attached to the wall. The average behavior indicates that, despite the low value close to the wall, the probability remains almost uniform with a depression in the central core likely related to a complementary increase in gas holdup all over the column (except in the upper region, see z/D = 7), as generally observed for recirculation patterns driven by bubble swarms [28–30]. Around the disengagement region the tracer occurrences near the column center increase, arising likely from a fountain type circulation of the solids associated to big bubbles bursts. The solid is released from the bubbles wakes, it is expelled towards the wall and finally accumulates and descend mostly in an annulus (r/R ∼ 0.7–0.9), where the highest solid occurrences appear; i.e., in an outer ring but separated from the wall.

The probability of the solid occurrence is related to the solid holdup [15,25]; multiplied by the global solid holdup would provide and estimation of the local solid holdup. As the solid inventory is the same for all the experiments, the global solid holdup decreased as the gas velocity is increased, and can be estimated from the uppermost axial values of the tracer.

The gas holdup profile was found to be distinctly affected by the foaming features of the liquid in bubble columns, depending on the column height and, in the entrance zone, on the type of gas distributor used [31,32].

Along the axial coordinate, a decrease in the solid probability was found for all the experimental conditions, in coincidence with information reported in the literature and in accordance with the generally proposed sedimentation dispersion models for three-phase bubble columns [15,33].

From the long trajectory of the solid tracer, residence time distribution (RTD) of the particles for given regions can be determined. Whenever the particle enters the zone of interest, the time that the tracer remains inside is computed. In this way, the RTD can be constructed provided the number of entering events is large enough (e.g., more than 100) to have good statistics. From RTDs at different column regions, the mean residence time of the solid all over the column

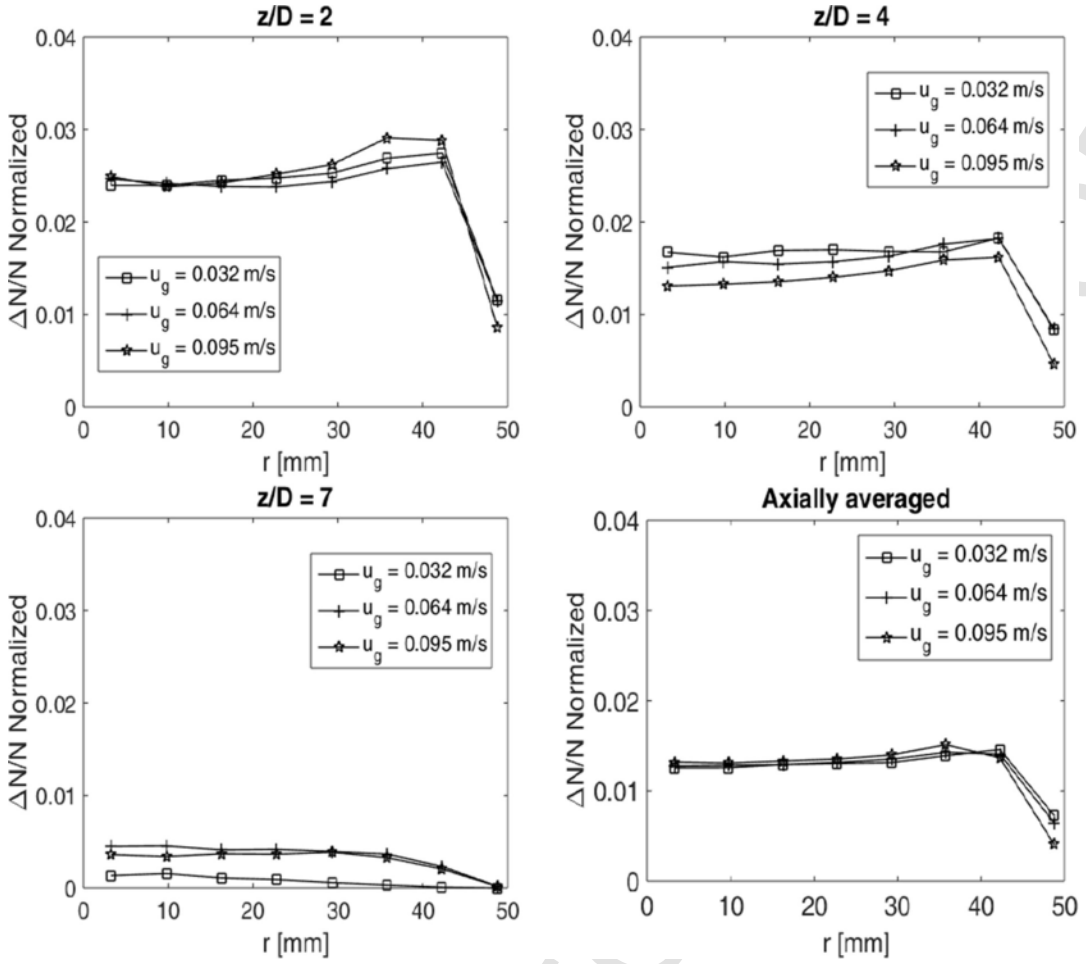

Fig. 2. Volume normalized probability of finding the tracer as a function of the radial coordinate, for representative gas velocities at different column heights and axially averaged. Lines are only to guide the eyes.

can be estimated. Fig. 3 illustrates radial-axial maps of solid mean residence times for representative experiments.

The tracer moves throughout the whole column, but preferentially remains slightly longer periods close to the entrance zone and for radial positions separated from the center and the wall. Longer residence times are generally because the particles are moving with no definite direction or they are trapped in local vortical structures. Residence times of the tracer in the column center or close to the disengagement region are generally shorter.

The solid mean flow pattern for three representative gas velocities corresponding to the bubbling and the churn-turbulent flow regimes, and for a condition around the transition, are shown in Fig. 4. Time and azimuthally averaged (considering axisymmetry) particle radial and axial velocities are represented on the radial-axial plane.

Two circulation cells are evident for low gas velocities, while they apparently collapse into one cell covering the whole column as the gas velocity increases. Similar behavior has been found for three phase bubble columns with solids of different sizes and a larger density ratio with respect to the liquid [15,16]. The typical behavior has also been found in the same facility while working in non-foaming systems with activated carbon as the solid phase [23]. The solid in this work has a density only slightly higher than the liquid phase density; hence, the solid motion has less inertia and it likely follows more strongly the liquid flow than denser particles.

The entrance circulation cell observed at low gas velocities extends for a height of about z/D ~ 1 (D is the column diameter). The second circulation cell extends through the rest of the column height, even if minor subcells can be perceived by observing the pattern close to the wall, resembling the multiple circulation cells coming from transient coherent structures interpreted by Joshi et al. [26]. For higher gas velocities, the multiple circulation cells can still be perceived in the mean flow pattern, and the vortical flow structures superimposed to a meandering central bubble plume, observed by Chen et al. [27] for two-phase bubble columns, can also be inferred from the tracer jittery trajectory. In a time-averaged representation, a gross scale single cell circulation, with upward flow in the central part of the column and downward-inwards flow in the wall region is observed.

Comparing with previous studies with denser particles and non-foaming liquids, in this case there is an evident inwards radial flow all over the column wall, highlighted in the axially averaged flow field represented on the transversal plane in Fig. 5 (note the scale enlargement).

This marked inwards flow could be related to the strong adherence to the wall of the foaming gas-liquid emulsion, which would prevent the solid to stay at radial positions larger than r/R ~ 0.9 (R is the column radius). Naturally, also the tracer size prevents the particle to be at radial positions larger than its radius (i.e., r/R > 0.95). The presence of foam creeping at the wall is visually observed and appar-

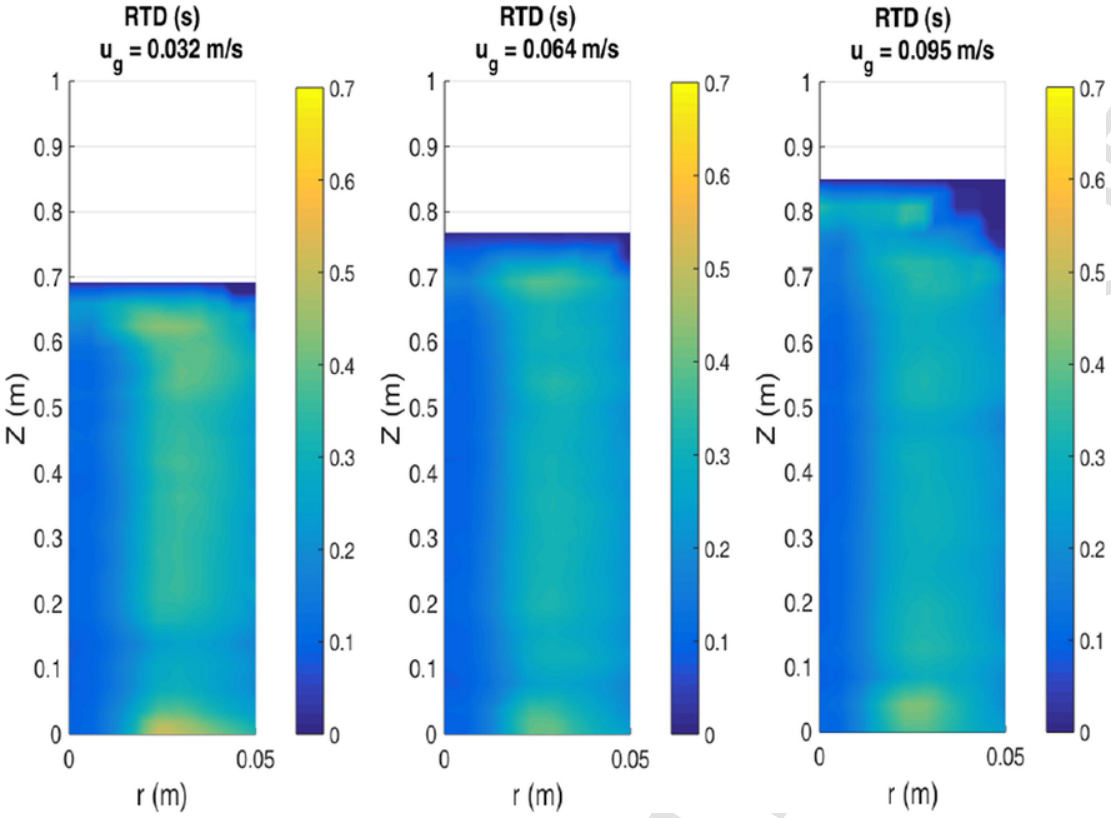

Fig. 3. Distribution of the solid mean residence time at different column regions for representative gas velocities.

ently occasions a hindrance effect. The descending solid motion close to the wall is less defined than in systems without foam; the motion is mostly inwards and only slightly descending. It is worthwhile mentioning that, even if the solid expansion does not surpass 0.8 m, the foam usually creeps towards the top of the 1.2 m column, especially for high aeration.

Radial profiles of the mean solid axial and radial velocities (azimuthally averaged) are shown, for different gas velocities, in Figs. 6 and 7, respectively. Velocities are shown for given axial locations, and axially averaged.

Solid axial velocities are generally positive in the central region and negative close to the wall, except for the lowest gas velocity close to the gas distributor. The inversion point is around $r/R \sim 0.6$, in coincidence with reports from previous works for three-phase bubble columns [15,16,18,28,34]. However, in contrast to what is generally observed for non-foaming systems, even in the same facility, the solid velocity for the region very close to the wall is less negative and can even change direction. Moreover, axial velocities attain minimum values for $r/R \sim 0.9$, for several axial positions. This behavior could be related to the hindrance and damping effect of the foam [35,36]. It has been recently shown that for the churn and annular flow regimes of a foaming gas-liquid system in a vertical pipe, the usually descending liquid film adjacent to the wall turns to an ascending or not definitely descending gas-liquid emulsion film [36,37].

The radial velocities, shown in Fig. 7 for the same conditions, are close to zero within the central core and become increasingly negative for radius close to the wall for most of the axial positions, indicating a relatively important inwards flow, which was not found in previous works. An outer flow can be observed only close to the disengagement region and in the limit of circulation subcells. Differences with previous information could be attributed to the foaming characteristics of the system and the low density and deformability of the particles.

Axial and radial velocities increase in absolute value as the gas velocity increases, in agreement with reports from previous works.

3.2. Turbulence characteristics

The magnitudes of the fluid hydraulic forces are important for bioreactor design and operation. High turbulent stresses can cause damage to cells and should preferably be avoided. Proper mapping of the regions of high shear stress is thus helpful for the successful design of bioreactors [19]. The time and azimuthally-averaged Reynolds radial-axial shear-stresses, calculated from the solid tracer fluctuating velocities, are mapped onto the radial-axial plane for three representative gas velocities in Fig. 8.

Solids shear stress has been related to the radial gradient of axial velocity in two and three phase bubble columns and, therefore, the maximum was generally coincident with the axial velocity inversion radius [17,18,34,38]. An increase in superficial gas velocity increases the solids axial velocity, and also its gradient, resulting in higher shear stresses at higher superficial gas velocities. For this system, the shear stress is more intense in the region close to the column center for all the experimental conditions. For low gas velocities, it is apparently low all over the column although it is slightly higher in the column core at the entrance and in the disengagement region. As gas velocities increases, the region of high share close to the column center becomes wider. For the churn turbulent flow regime, the shear close to the disengagement zone becomes significantly more intense in spite of the damping effect of the foam.

Fig. 9 illustrates the radial dependence of the axial and azimuthally averaged shear stresses for representative gas velocities.

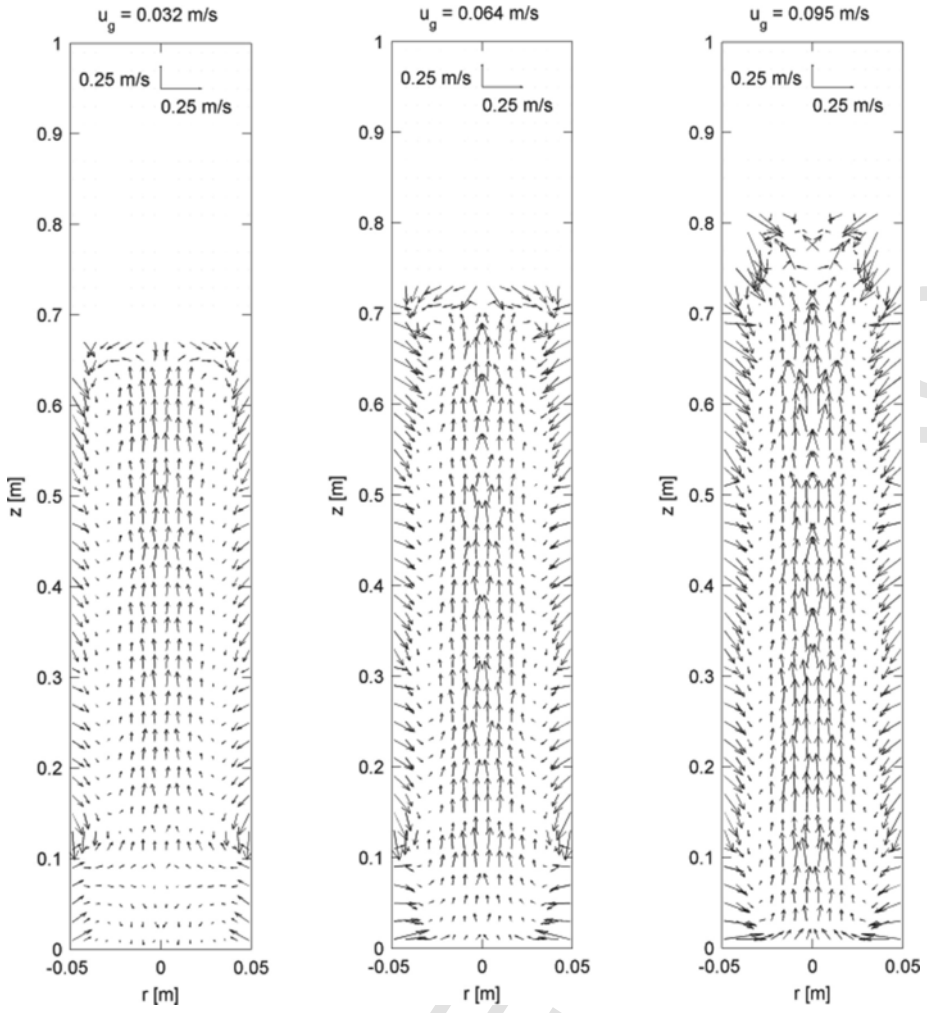

Fig. 4. Axial-radial velocity fields (azimuthally averaged) for gas velocities representative of the bubbling, transition and churn-turbulent flow regimes.

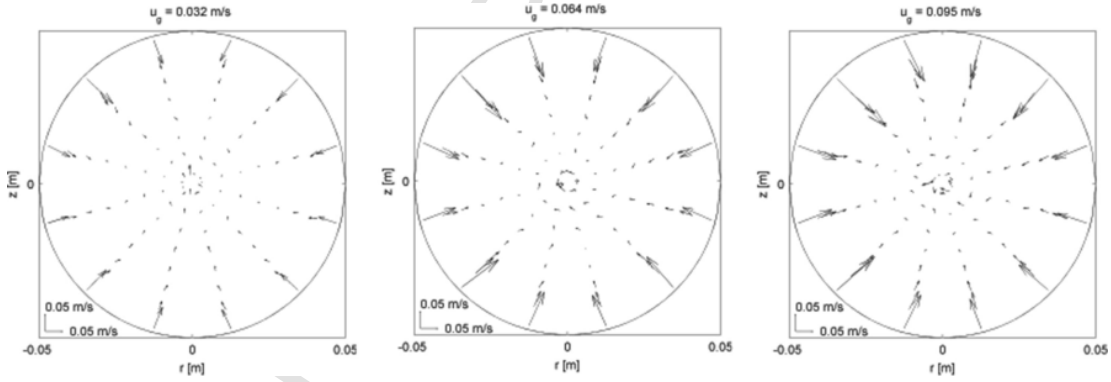

Fig. 5. Velocity fields (axially averaged) on the transversal plane for gas velocities representative of the bubbling, transition and churn-turbulent flow regimes.

Compared with results reported for bubble columns in non-foaming systems [24], it comes out that the shear in foaming systems are around half the values measured in a gas-liquid bubble column without foam.

The zone of highest values is closer to the column center than in bubble columns without foam and significantly influenced by the change in flow regime. The maximum shear displaced towards the column center observed in this work could probably be related to the very definite inward flow of the solid close to the wall, which would prevent the solely dependence on the solid axial velocity gradient.

The time and azimuthally-averaged turbulent kinetic energies (normal stresses), calculated from the solid tracer fluctuating velocities, are mapped onto the radial-axial plane for three representative gas velocities in Fig. 10.

The turbulent kinetic energy (TKE) distribution is reasonably homogeneous, increasing in the lowest region of the column and, espe-

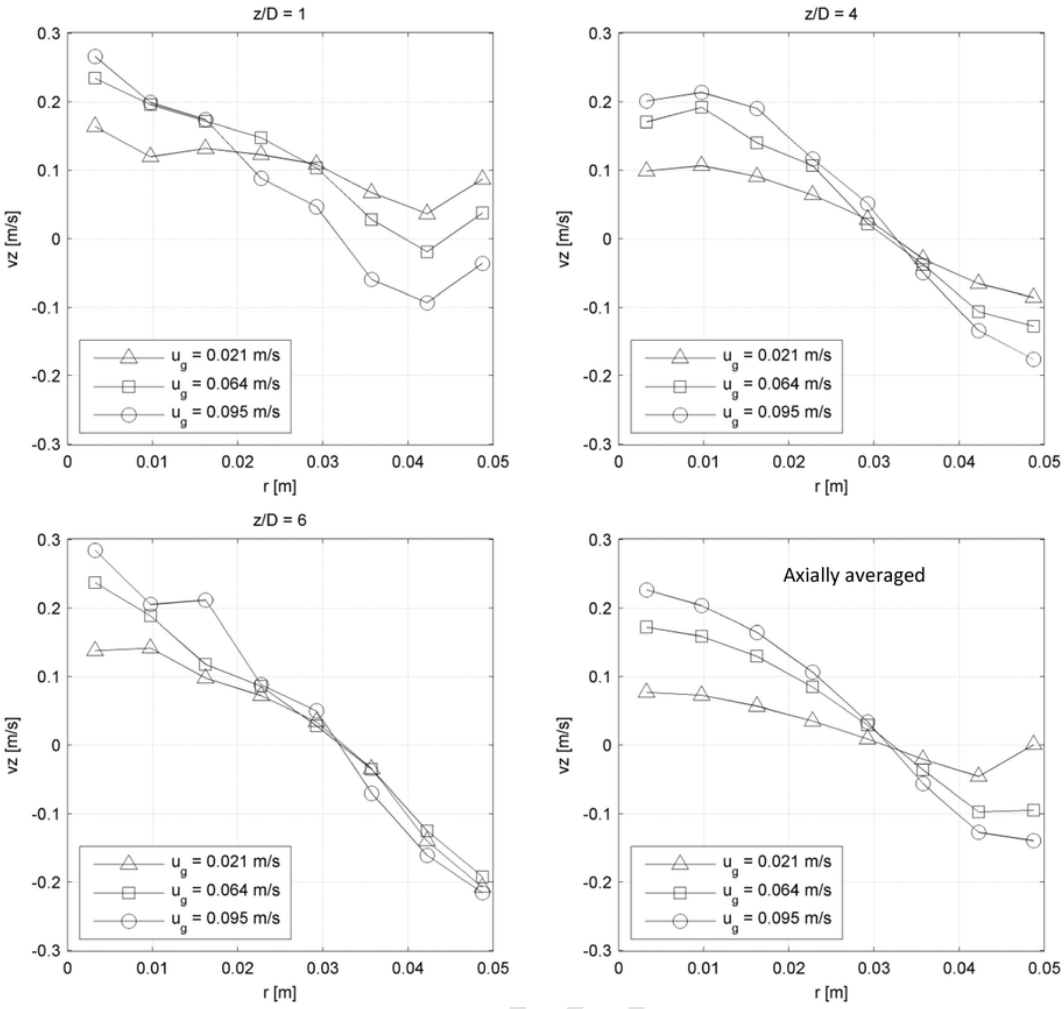

Fig. 6. Azimuthally averaged solid axial velocities as a function of the radial coordinate for different gas velocities at given column heights and axially averaged. Lines are only to guide the eyes.

cially for low gas velocities, locally in the region where the circulation cell direction change is observed in the velocity field. For high gas velocities, TKE is quite larger in the upper region of the column, being maximum around the disengagement zone and for locations where the dimensionless radius is less than the one leading to axial velocity inversion ($r/R \sim 0.6$). These results are comparable with information from the literature for two and three phase bubble columns within the totally developed region [15,17,19,34,39].

The TKE and shear stress maximum values found in this system are strongly dependent on gas velocity. Maximum local shear stresses are around 10 N/m^2 while the maximum TKE can reach values of 250 N/m^2 for certain regions at low gas velocities, and even higher than 450 N/m^2 in the disengagement region, for high gas velocities. The highest values are possibly related to the vortical structures induced by circulating bubble swarms, and by the bubble bursts around the disengagement region, for experiments in the heterogeneous flow regime. Within the bubbling flow regime, the turbulent stresses are generally lower than 100 N/m^2 all over the reactor, except close to the entrance zone, where the gas injection generates important friction.

Turbulent stresses are responsible for the hydrodynamic stress suffered by the biocatalysts in bioreactors, cell damage in bioreactors is assumed to occur when local shearing stresses exceed a threshold. However, it is difficult to decide the threshold level to consider. The maximum measured in the maps can be taken into account to quantify it; however, maximum local values can probably overestimate the risk of damage since the heterogeneity is generally large. On the contrary, mean values could be too low since a non-weighted average would take into account even almost stagnant regions of the column. Another factor that should be considered is the frequency with which the cells are exposed to regions of large stress. Some of the column regions are seldom visited by the particles and, therefore, even if they have large stress, they may not have large influence [40]. From RPT experiments, the frequency of visit of different column regions can be evaluated as the inverse of the mean time elapsed before the tracer reenters given locations. By evaluating these periods, it is apparent that the particles circulate more frequently in the lower part of the column and are rarely close to bubbles burst. As recently suggested by Liu et al. [40], the product of the stresses and the frequency of visit would provide more reliable estimation of the risk of damage to which the organisms are exposed. Maps of exposure to the shear and normal stresses are presented in Fig. 11. From these maps, it is apparent that the highest exposure risks are in the order of 10–15 W/m^3 and they are located in the lower region of the column, close to the gas entrance. Therefore, particular attention should be given to the gas distributor design to avoid excessive turbulence in this zone.

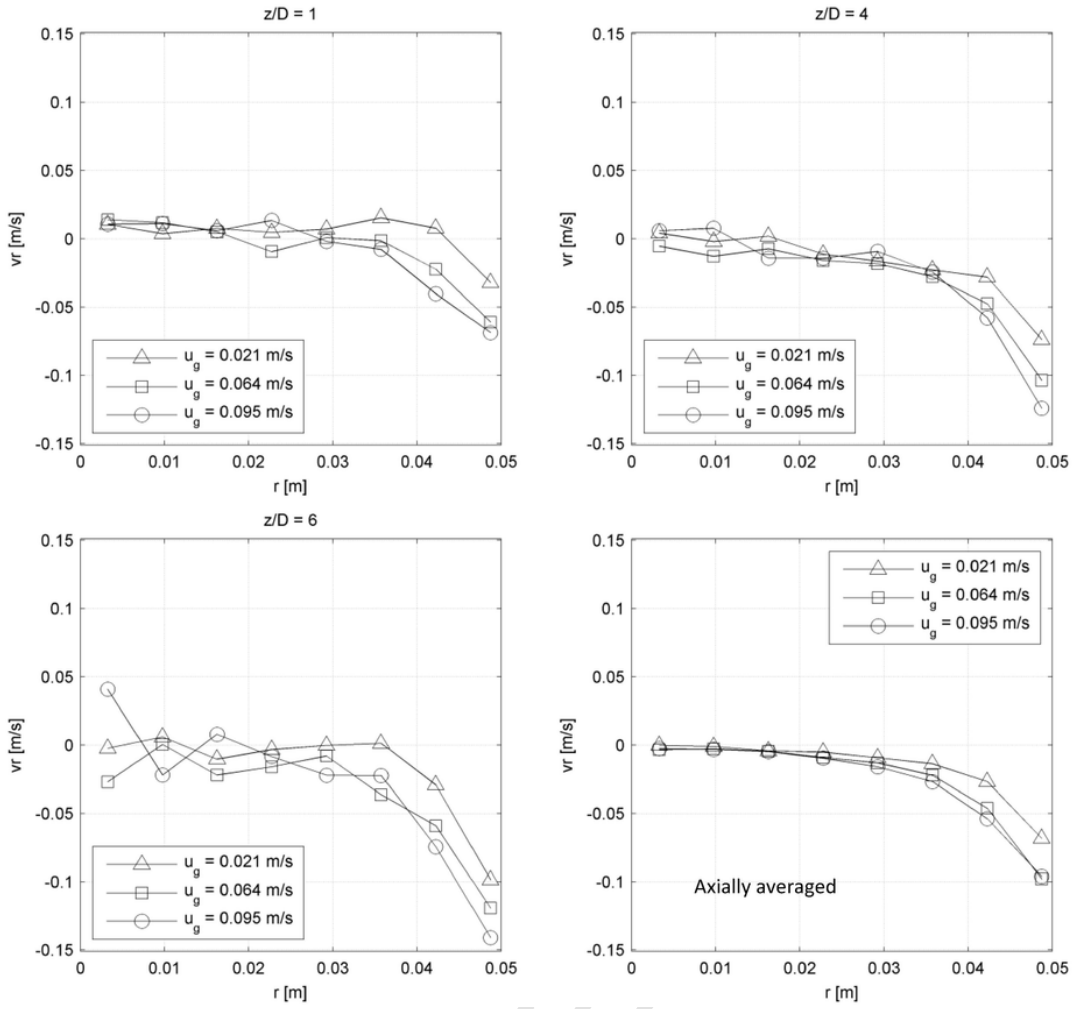

Fig. 7. Azimuthally averaged solid radial velocities as a function of the radial coordinate for different gas velocities at given column heights and axially averaged. Lines are only to guide the eyes.

3.3. Solid dispersion coefficients

From a Lagrangian viewpoint, the radial and axial dispersion coefficients can also be calculated from the long tracer trajectory assuming ergodicity, by considering the time dependence of the mean square displacements after the initial correlation time [34]. Radial and axial dispersion coefficients have therefore been calculated for the examined experimental conditions from the variance of particle trajectories starting from different regions in the column. The influence of gas velocity on dispersion coefficients is illustrated in Fig. 12. Values are obtained as the mean resulting from initial points at different locations all around the column and the error bar indicates variations among results starting at different positions. The positive influence of gas velocity is larger than the influence of the starting point. The order of magnitude and the gas velocity dependence is comparable to results reported in the literature for other type of solid in three phase bubble columns with gas and liquid flow [34,41]. The order of magnitude is also similar to those measured in bubble columns with RPT [24] but the values are around half probably due to a dumping effect of the foam.

The increase in dispersion coefficients with gas velocity is approximately linear within the bubbling flow regime, decreasing the positive trend after the transition to the churn turbulent flow regime. Axial dispersion coefficients are about an order of magnitude larger than the radial ones, also in accordance with previous findings for non-foaming liquids in gas-liquid and three-phase bubble columns [24,34].

4. Conclusions

Relevant information about the motion of calcium alginate beads in a three-phase bubble column with a foaming gas-liquid system has been obtained from Radioactive Particle Tracking experiments. Solid axial and radial velocities and turbulence stresses have been found to be markedly dependent on gas velocity. For this foaming system, axial flow is dominantly positive in the column core and negative in the annulus region. However, a marked inwards flow and less negative axial velocities have been determined very close to the wall likely related to the foam, which tends to adhere to column wall preventing a descending liquid film.

The most intense turbulent forces are found in the column core and particularly in the disengagement region for the churn turbulent flow regime. Maximum local shear stresses are around 10 N/m^2 which are significantly lower (less than half the values) than those characterizing bubble columns without foam. The maximum TKE

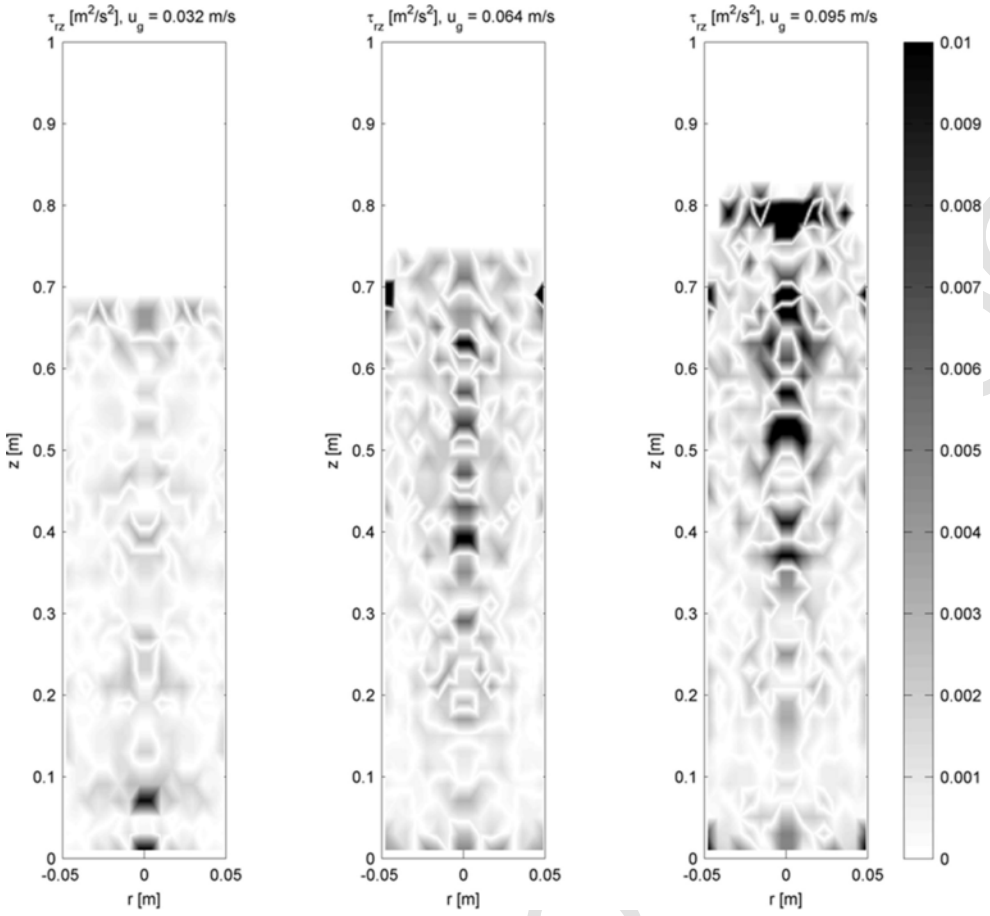

Fig. 8. Visualization of time- and azimuthally-averaged radial-axial shear stress in the radial-axial plane for experimental conditions representative of the bubbling and the churn-turbulent flow regimes.

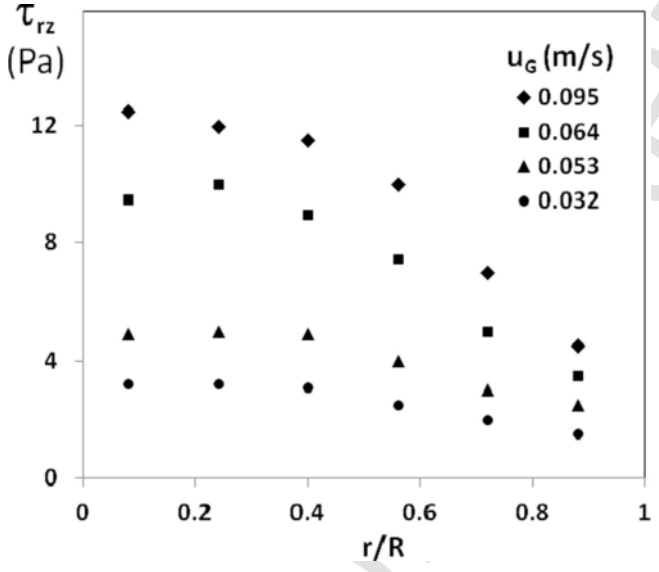

Fig. 9. Radial dependence of the axial and azimuthally averaged shear stresses, for representative gas velocities.

(normal stresses) can reach values higher than 450 N/m^2 in the disengagement region, for high gas velocities. Within the bubbling flow regime, the TKE are lower than 100 N/m^2 all over the reactor, except close to the entrance zone, where the gas injection generates important friction and TKE more than doubles. Shear stresses may reach the same values as for high gas velocities close to the gas entrance. Even if the disengagement region shows the highest turbulence stresses, the frequency of finding the tracer in that region is very low for the calcium alginate beads representing immobilized biocatalysts. The product of the stresses and this frequency would be a better indicator of the zones of highest risk for biocatalysts damage. Considering this product, it is found that the largest risks are located close to the gas entrance indicating that particular attention must be given to design of gas distributors in order to minimize the turbulence arising from gas friction in the injection points.

Solid axial and radial dispersion coefficients increase with gas velocity with an approximately linear trend within the bubbling flow regime. The positive trend decrease after the inception of the churn-turbulent flow regime.

Acknowledgments

Financial support from FonCyT (PICT2014-0704) and Universidad de Buenos Aires (UBACyT 20020130100544BA) are gratefully acknowledged. G. Salierno, M. Maestri, M. Cassanello, M.A. Cardona and D. Hojman are members of CONICET. We would particularly like to thank the staff of the RA1 reactor of CNEA, Argentina, for the activation of the sources used in this work.

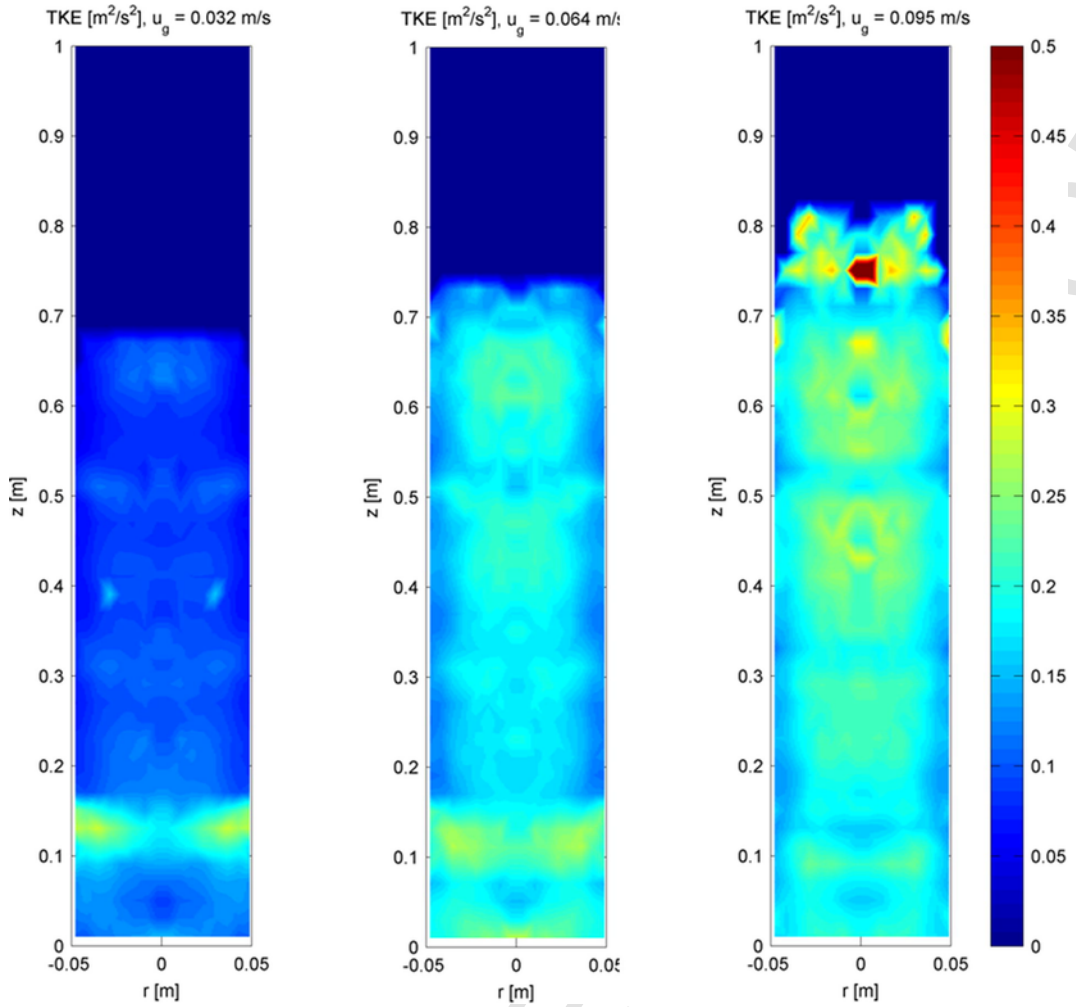

Fig. 10. Visualization of time- and azimuthally-averaged turbulent kinetic energy in the radial-axial plane for experimental conditions representative of the bubbling and the churn-turbulent flow regimes.

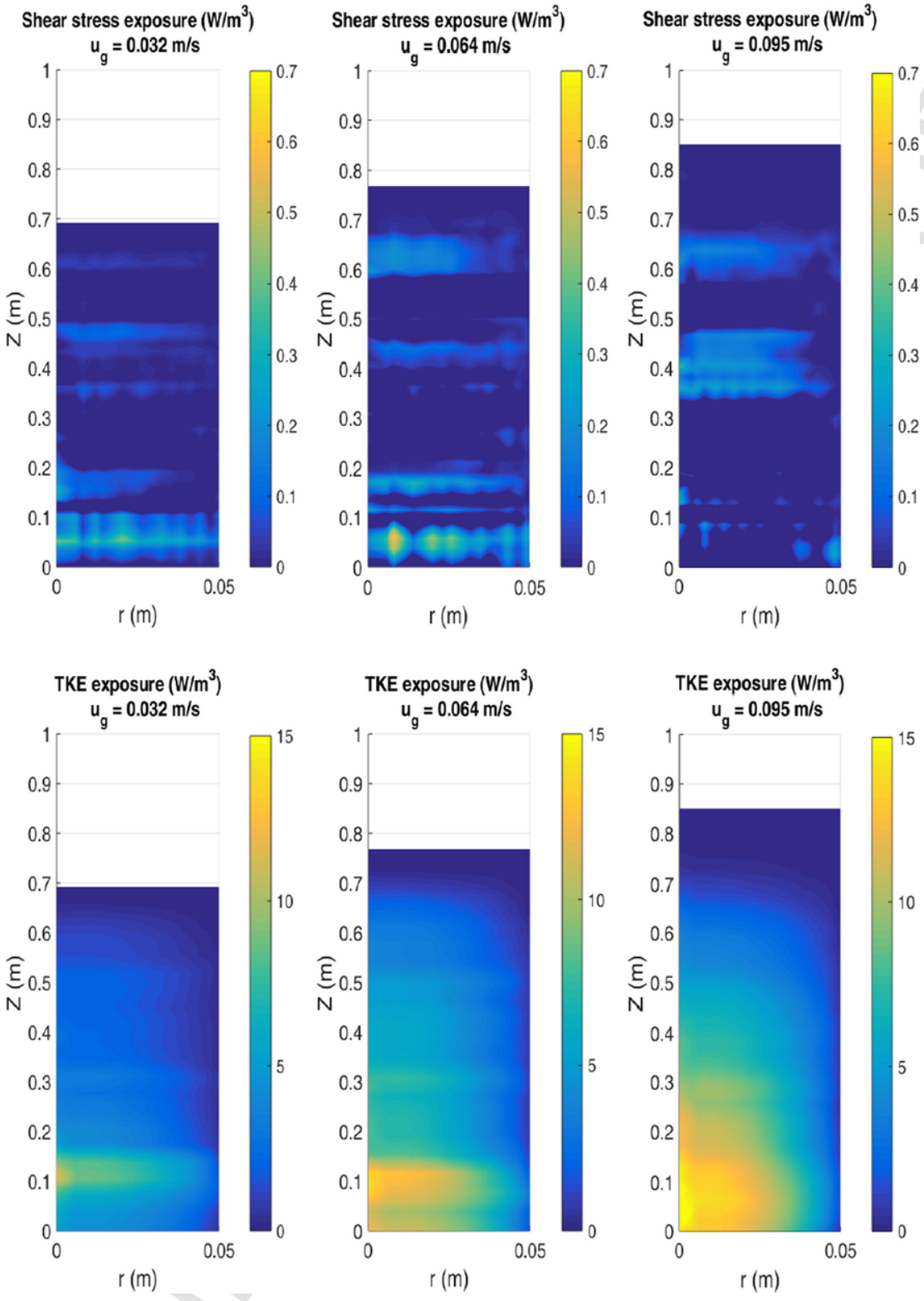

Fig. 11. Risk of biocatalysts damage exposure evaluated as the product of the stress and the frequency of visit of the tracer at different column regions.

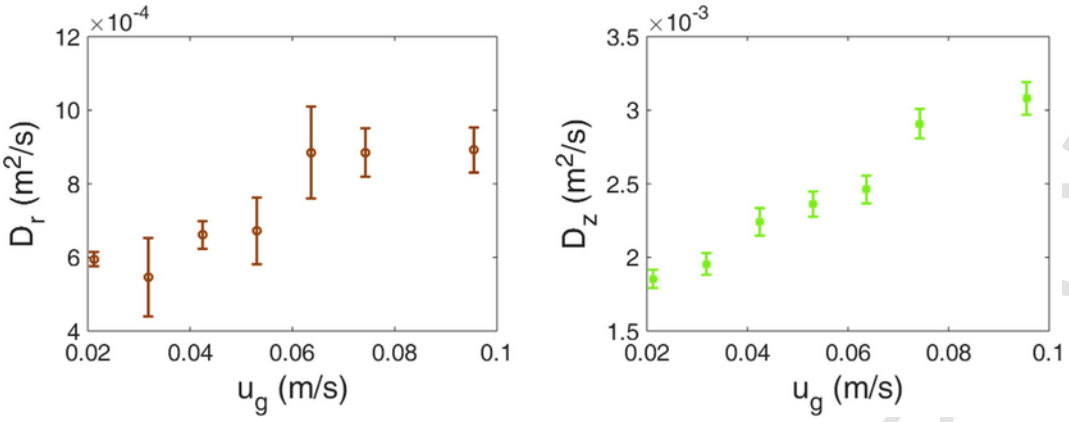

Fig. 12. Solid radial (left) and axial (right) dispersion coefficients as a function of gas velocity.

References

[1] S. Gabardo, R. Rech, C.A. Rosa, M.A. Záchia Ayub, Dynamics of ethanol production from whey and whey permeate by immobilized strains of Kluyveromyces marxianus in batch and continuous bioreactors, Renewable Energy 69 (2014) 89–96.

[2] B. Pérez-Bibbins, R. Pinheiro de Souza Oliveira, A. Torrado, M.G. Aguilar-Uscanga, J.M. Domínguez, Study of the potential of the air lift bioreactor for xylitol production in fed-batch cultures by Debaryomyces hansenii immobilized in alginate beads, Appl. Microbiol. Biotechnol. 98 (2014) 151–161.

[3] B. Lee, P. Ravindra, E. Chan, Size and shape of calcium alginate beads produced by extrusion dripping, Chem. Eng. Technol. 36 (2013) 1627–1642.

[4] N. Kantarci, F. Borak, K.O. Ulgen, Bubble column reactors, Process Biochem. 40 (2005) 2263–2283.

[5] A. Pandey, C. Larroche, S.C. Ricke, C.-G. Dussap, E. Gnansounou, Biofuels: Alternative Feedstocks and Conversion Processes, Academic Press, Oxford UK, 2013.

[6] S.J. Parulekar, P.V. Shertukde, J.B. Joshi, Underutilization of bubble column reactors due to desorption, Chem. Eng. Sci. 44 (1989) 543–558.

[7] M.L. Collignon, A. Delafosse, M. Crine, D. Toye, Axial impeller selection for anchorage dependent animal cell culture in stirred bioreactors: methodology based on the impeller comparison at just-suspended speed of rotation, Chem. Eng. Sci. 65 (2010) 5929–5941.

[8] R.M. Shenkman, R. Godoy-Silva, K.K. Papas, J.J. Chalmers, Effects of energy dissipation rate on islets of langerhans: implications for isolation and transplantation, Biotechnol. Bioeng. 103 (2009) 413–423.

[9] C.H. Tan, P.L. Show, J.-S. Chang, T.C. Ling, J.C.-W. Lan, Novel approaches of producing bioenergies from microalgae: a recent review, Biotechnol. Adv. 33 (2015) 1219–1227.

[10] L. Beckers, J. Masset, C. Hamilton, F. Delvigne, D. Toye, M. Crine, P. Thonart, S. Hiligsmann, Investigation of the links between mass transfer conditions, dissolved hydrogen concentration and biohydrogen production by the pure strain Clostridium butyricum CWBI1009, Biochem. Eng. J. 98 (2015) 18–28.

[11] J.J. Chalmers, Mixing, aeration and cell damage, 30+ years later: what we learned, how it affected the cell culture industry and what we would like to know more about, Curr. Opin. Chem. Eng. 10 (2015) 94–102.

[12] M. Moo-Young, M. Butler, C. Webb, A. Moreira, B. Grodzinski, Z.F. Cui, S. Agathos, Comprehensive Biotechnology, second ed., Elsevier, 2011.

[13] J.S. Guez, S. Chenikher, J.Ph. Cassar, P. Jacques, Setting up and modelling of overflowing fed-batch cultures of Bacillus subtilis for the production and continuous removal of lipopeptides, J. Biotechnol. 131 (2007) 67–75.

[14] S. Yao, S. Zhao, Z. Lu, Y. Gao, F. Lv, X. Bie, Control of agitation and aeration rates in the production of surfactin in foam overflowing fed-batch culture with industrial fermentation, Rev. Argent. Microbiol. 47 (2015) 344–349.

[15] S. Grevskott, B.H. Sannaes, M.P. Dudukovic, K.W. Hjarbo, H.F. Svendsen, Liquid circulation, bubble size distributions, and solids movement in two- and three-phase bubble columns, Chem. Eng. Sci. 51 (1996) 1703–1713.

[16] F. Larachi, M. Cassanello, J. Chaouki, C. Guy, Flow structure of the solids in a 3-D gas-liquid-solid fluidized bed, AIChE J. 42 (1996) 2439–2452.

[17] S. Degaleesan, M.P. Dudukovic, Y. Pan, Experimental study of gas-induced liquid-flow structures in bubble columns, AIChE J. 47 (2001) 1913–1931.

[18] N. Rados, A. Shaikh, M.H. Al-Dahhan, Solids flow mapping in a high pressure slurry bubble column, Chem. Eng. Sci. 60 (2005) 6067–6072.

[19] H.-P. Luo, M.H. Al-Dahhan, Local characteristics of hydrodynamics in draft tube airlift bioreactor, Chem. Eng. Sci. 63 (2008) 3057–3068.

[20] H.-P. Luo, M.H. Al-Dahhan, Airlift column photobioreactors for Porphyridium sp. culturing: Part I. Effects of hydrodynamics and reactor geometry, Biotechnol. Bioeng. 109 (2012) 932–941.

[21] M. Vesvikar, M.H. Al-Dahhan, Hydrodynamics investigation of laboratory-scale internal gas-lift loop anaerobic digester using non-invasive CAPRT technique, Biomass Bioenergy 84 (2016) 98–106.

[22] C. Haringa, W. Tang, A.T. Deshmukh, J. Xia, M. Reuss, J.J. Heijnen, R.F. Mudde, H.J. Noorman, Euler-Lagrange computational fluid dynamics for (bio)reactor scale down: an analysis of organism lifelines, Eng. Life Sci. 16 (2016) 652–663.

[23] G. Salierno, Caracterización de equipos y medios multifásicos con métodos que emplean fuentes radiactivas (Ph.D. thesis), Universidad de Buenos Aires, Argentina, 2016. <http://digital.bl.fcen.uba.ar/Download/Tesis/Tesis_5951_Salierno.pdf>.

[24] J. Chaouki, F. Larachi, M.P. Dudukovic, Non-Invasive Monitoring of Multiphase Flows, Elsevier, 1997.

[25] G. Salierno, M.S. Fraguío, S. Piovano, M. Cassanello, M.A. Cardona, D. Hojman, H. Somacal, Bubble columns dynamics inferred from the motion of a radioactive tracer followed by axially aligned detectors, Chem. Eng. J. 207–208 (2012) 450–461.

[26] J.B. Joshi, V.S. Vitankar, A.A. Kulkarni, M.T. Dhotre, K. Ekambara, Review paper: coherent flow structures in bubble column reactors, Chem. Eng. Sci. 57 (2002) 3157–3183.

[27] R.C. Chen, J. Reese, L.-S. Fan, Flow structure in a three-dimensional column and three-phase fluidized bubble bed, AIChE J. 40 (1994) 1093–1104.

[28] Z.W. Gan, Holdup and velocity profiles of monosized spherical solids in a three-phase bubble column, Chem. Eng. Sci. 94 (2013) 291–301.

[29] S. Rabha, M. Schubert, U. Hampel, Intrinsic flow behavior in a slurry bubble column: a study on the effect of particle size, Chem. Eng. Sci. 93 (2013) 401–411.

[30] S. Rabha, M. Schubert, M. Wagner, D. Lucas, U. Hampel, Bubble size and radial gas hold-up distributions in a slurry bubble column using ultrafast electron beam X-ray tomography, AIChE J. 59 (2013) 1709–1722.

[31] U. Parasu Veera, K. Kataria, J.B. Joshi, Effect of superficial gas velocity on gas hold-up profiles in foaming liquids in bubble column reactors, Chem. Eng. J. 99 (2004) 53–58.

[32] U. Parasu Veera, K.L. Kataria, J.B. Joshi, Gas hold-up in foaming liquids in bubble columns, Chem. Eng. J. 84 (2001) 247–256.

[33] W.-T. Tang, L.-S. Fan, Hydrodynamics of a three-phase fluidized bed containing low-density particles, AIChE J. 35 (1989) 355–364.

[34] K. Kiared, F. Larachi, J. Chaouki, C. Guy, Mean & turbulent particle velocity in the fully developed region of a three-phase fluidized bed, Chem. Eng. Technol. 22 (1999) 683–689.

[35] A. Sauret, F. Boulogne, J. Cappello, E. Dressaire, H.A. Stone, Damping of liquid sloshing by foams, Phys. Fluids 27 (2015). 022103-1–022103-15.

[36] A.T. van Nimwegen, L.M. Portela, R.A.W.M. Henkes, The effect of surfactants on air–water annular and churn flow in vertical pipes. Part 1: Morphology of the air–water interface, Int. J. Multiphase Flow 71 (2015) 133–145.

[37] A.T. van Nimwegen, L.M. Portela, R.A.W.M. Henkes, The effect of surfactants on air–water annular and churn flow in vertical pipes. Part 2: Liquid holdup and pressure gradient dynamics, Int. J. Multiphase Flow 71 (2015) 146–158.

[38] R.F. Mudde, D.J. Lee, J. Reese, L.-S. Fan, Role of coherent structures on reynolds stresses in a 2-D bubble column, AIChE J. 43 (2004) 913–926.

[39] Z. Cui, L.S. Fan, Turbulence energy distributions in bubbling gas–liquid and gas–liquid–solid flow systems, Chem. Eng. Sci. 59 (2004) 1755–1766.

[40] Y. Liu, Z.J. Wang, J. Xia, C. Haringa, Y. Liu, J. Chu, Y.-P. Zhuang, S.-L. Zhang, Application of Euler-Lagrange CFD for quantitative evaluating the ef-

fect of shear force on Carthamus tinctorius L. cell in a stirred tank bioreactor, Biochem. Eng. J. 114 (2016) 209–217.
[41] H.O. Lim, M.J. Seo, Y. Kang, K.W. Jun, Particle fluctuations and dispersion in three-phase fluidized beds with viscous and low surface tension media, Chem. Eng. Sci. 66 (2011) 3234–3242.